

Received 20 April 2020; revised 24 June 2020; accepted 21 July 2020. Date of publication 23 July 2020; date of current version 7 August 2020.
The review of this article was arranged by Editor J.-S. Goo.

Digital Object Identifier 10.1109/JEDS.2020.3011635

Parameter Extraction for the PSPHV LDMOS Transistor Model

KEJUN XIA^{ID} (Senior Member, IEEE), COLIN C. MCANDREW^{ID} (Fellow, IEEE),
AND RONALD VAN LANGEVELDE^{ID} (Member, IEEE)

Department of Front End Innovation, NXP Semiconductors N. V., Chandler, AZ 85224, USA

CORRESPONDING AUTHOR: K. XIA (e-mail: kejun.xia@nxp.com)

ABSTRACT This paper details a robust parameter extraction flow for the PSPHV LDMOS transistor model. The procedure uses a global scaling parameter set and accounts for self-heating. We describe how to determine parameters associated with important physical effects specific to PSPHV: non-uniform lateral channel doping; the Kirk effect; internal drain voltage clamping; and the drain expansion effect. The method is verified on devices from different technologies. Verilog-A code for PSPHV is publicly available.

INDEX TERMS MOSFET, LDMOS, parameter extraction, semiconductor device modeling, SPICE.

I. INTRODUCTION

Laterally diffused MOS (LDMOS) transistors are widely used in integrated circuits (ICs) for applications such as switch-mode power supplies, power amplifiers, power management, and motor drivers. Recently, we developed an accurate surface-potential based compact LDMOS transistor model PSPHV [1] to help design and optimize such ICs. PSPHV consists of an enhanced version of the PSP103.6 MOS transistor model [2] for the intrinsic channel, a modified version of the JFETIDG dual-gate JFET model [3] for the drift region, and JUNCAP2 [4], extended to improve modeling at high forward bias, for parasitic junction diodes. These components are integrated into a single Verilog-A code which is publicly available [5].

Compared to existing compact models for LDMOS transistors, such as SPHV [6], BSIM-HV [7], and the CMC standard model HiSIM_HV [8], PSPHV:

- models nonuniform lateral doping (NULD), from out-diffused channels and source-side halo implants
- models gradual channel turn-on
- does not exhibit unphysical spikes in capacitance versus voltage [9]–[12]
- includes a significantly more accurate avalanche current model, that accounts for the Kirk effect [13]
- as an option, can include reverse recovery modeling for the junction diodes.

A model is not useful without a procedure to extract parameters of the model to fit a wide variety of device types. The parameter extraction process for PSPHV is reasonably complex because LDMOS transistors are complex devices, hence PSPHV is a fairly complex model. This paper presents a robust extraction flow for PSPHV, to help modeling engineers use PSPHV for the devices they need to model. In particular, we introduce a self-heating effect (SHE) aware extraction flow. Previously proposed LDMOS model parameter extraction procedures, e.g., [14], determine values for temperature coefficients as a final step. However, output characteristics at the reference temperature T_r cannot be fitted without good values for temperature coefficients, because behavior at high gate bias V_{gs} and drain bias V_{ds} is affected by SHE. Our procedure improves on the prior art because it self-consistently accounts for SHE.

Our procedure includes extraction of capacitance parameters, but the focus is extraction of drain current parameters for full channel width and length scaling. We show the effect of parameters on capabilities unique to PSPHV: drain voltage scaling, the Kirk effect, internal drain voltage clamping, and the drain expansion effect. Our method is verified using devices from different technologies. Extraction of parameters for other parts of the model, such as gate current, parasitic junction diodes, noise, etc. is not detailed here, and follows the procedures defined for PSP [2].

In some instances, there may be unexpected device characteristics that cause issues with using a “canned” extraction program on a new device. Our procedure recognizes this fact: below “extract” means either an initial manual tuning, or small optimization, of one or a small number of parameters to fit a limited set of data, and “optimization” means the step is more substantial, and not manual, and involves adjusting multiple parameters to fit multiple data sets, often over geometry and temperature as well as over bias.

II. OVERVIEW AND GLOBAL SWITCHES

PSPHV inherits the local-global hierarchical parameter structure of PSP [15]. Model parameters can be specified at a local level, i.e., for one specific geometry, or at a global level. Here we use global level parameters. All PSPHV parameters are in SI units and here are typeset in constantWidth font.

PSPHV can model LDMOS transistors with different drift region structures, see Fig. 1. For devices like those, set $swtgm\os = 1$ and $swbgm\os = 0$; this defines the type of the top and bottom gates of the drift region as MOS and p-n junction, respectively.

Fig. 2 shows the equivalent circuit for PSPHV (this includes parasitics series resistance not explicitly shown in [1]). The optional second gate-drain overlap capacitance is turned on by specifying a positive value for the instance parameter $lgdov2$, the length of the second gate-drain overlap region, see Fig. 1, (note that the bulk connection of this component is moved from the di to the d node compared to [1]; this improves accuracy).

For LDMOS transistor structures like those of Figs. 1(a) and 1(c), the first gate-drain overlap region, whose length is specified by the instance parameter $lgdov$, covers only a small portion of the overall drift region length. The JFETIDG model, which is used for the drift region, assumes that depletion pinching occurs over the whole length of that region (which is true for the bottom gate of the drift region, the bulk). If parameters for the JFETIDG top gate depletion pinching effect are extracted at low V_{ds} they unphysically predict the drift region will pinchoff at high V_{ds} . For such structures, set $dfto = 0$, to turn off the top gate depletion pinching effect, and instead model drift region resistance modulation by the top gate via the $mumto$ mobility modulation parameter.

For LDMOS transistor structures like Fig. 1(b), $lgdov$ covers a substantial portion of the drift region and the JFETIDG top gate depletion pinching model can be used. Initial estimates of top gate depletion pinching factor $dfto$ and built-in potential ψ_{rto} are

$$d_{fto} = \frac{\sqrt{\epsilon_s/(qN_c)}}{t_m + t_{ox}\epsilon_s/\epsilon_{ox}}, \quad \psi_{rto} = \frac{q\epsilon_s N_c t_{ox}^2}{\epsilon_{ox}^2} - 2V_{FB,ov} \quad (1)$$

where t_m is the drift region metallurgical thickness and t_{ox} is oxide thickness; ϵ_{ox} and ϵ_s are the permittivities of SiO₂ and Si, respectively, q is the magnitude of the electronic charge, N_c is the doping concentration in the drift region,

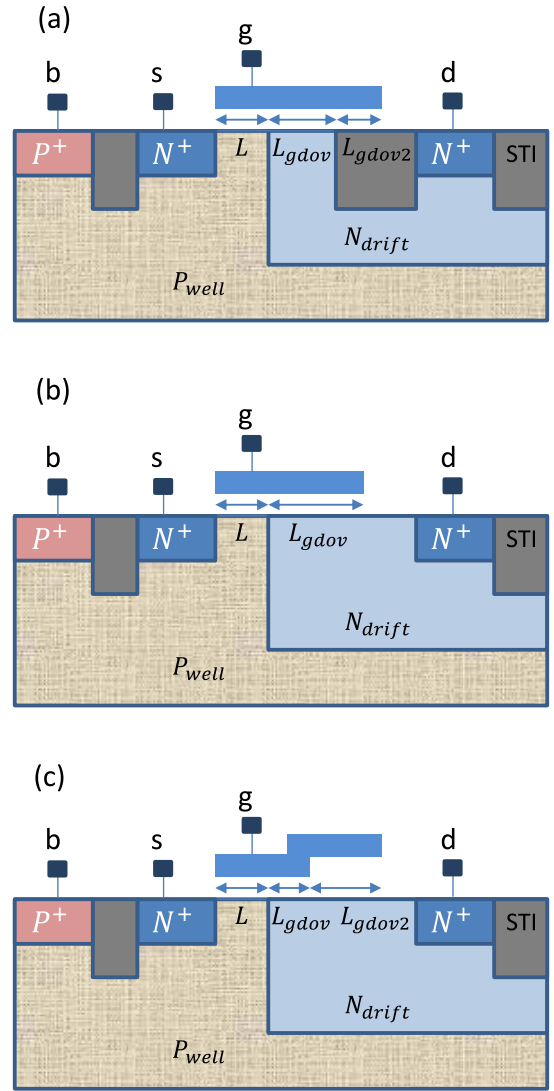


FIGURE 1. Cross-section of n-LDMOS transistors with different drift region designs.

assumed to be constant, and $V_{FB,ov}$ is the flat-band voltage of the overlap region.

Other important global switch settings:

- $swet$: set to 1 to turn on self-heating modeling (in which case either the thermal node must be connected to an external thermal network or the thermal resistance must be positive)
- $swvdscale$: set to 1 to turn on V_{ds} scaling to model NULD (this triggers a separate surface potential solution for charge calculations for the intrinsic MOS transistor, as when $swdelvtac = 1$)
- $swvdimp$: set to 1 to make PSP impact ionization calculations use $V(d,s)$ instead of $V(di,s)$ (this is necessary if V_{di} clamping is activated, when $swvdiclamp = 1$)
- $swdrlin$: set to 1 to have JFETIDG treat the drift region as a linear resistor (for debugging or to speed up simulations, with associated loss of accuracy of course)

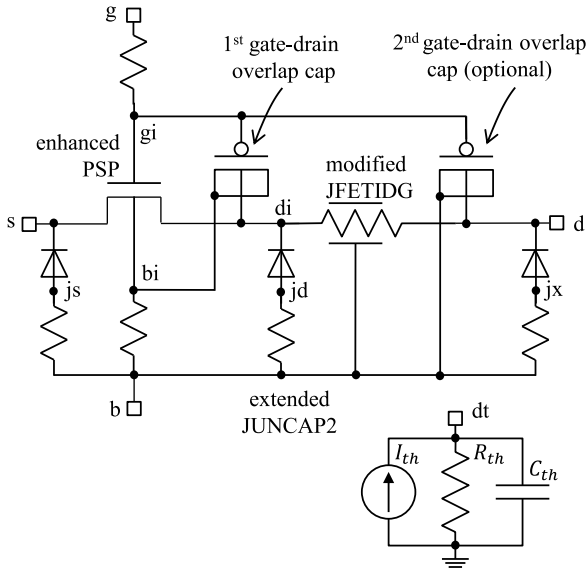


FIGURE 2. Large-signal equivalent circuit for PSPHV.

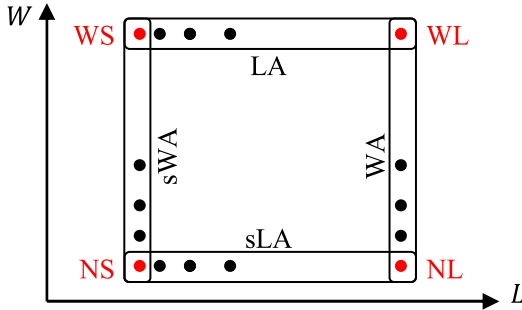


FIGURE 3. Device geometries for extraction.

- for swgeo, swedge, swigate, swimpact, swgidl, swjunc, swjunasym, swnud, and swdelvtac refer to the PSP manual [2]

III. DEVICE GEOMETRIES AND MEASUREMENTS

Figure 3 shows the device geometries that are needed to extract a fully scalable PSPHV model. WL, WS, NL, NS stand for the wide/long, wide/short, narrow/long, narrow/short devices, respectively. Besides the four corner geometries, there are primary and secondary width W and length L arrays. Because short and narrow channel effects vary roughly as $1/L$ and $1/W$, respectively, the length and width arrays should space geometries roughly equally in $1/L$ and $1/W$; this maximizes observability of parameters.

The following data are needed ($x = d, g, s, b$):

- DC data (all geometries and temperatures)
 - *idvg_lin*: $I_d(V_{gs})$ at low V_{ds} , over V_{bs} if the bulk and source are not tied together
 - *idvg_sat*: $I_d(V_{gs})$ and $I_b(V_{gs})$ at three or more high V_{ds} values and $V_{bs} = 0$
 - *idvd data*: $I_d(V_{ds})$ and $I_b(V_{ds})$ for several V_{gs} in strong inversion, $V_{bs} = 0$

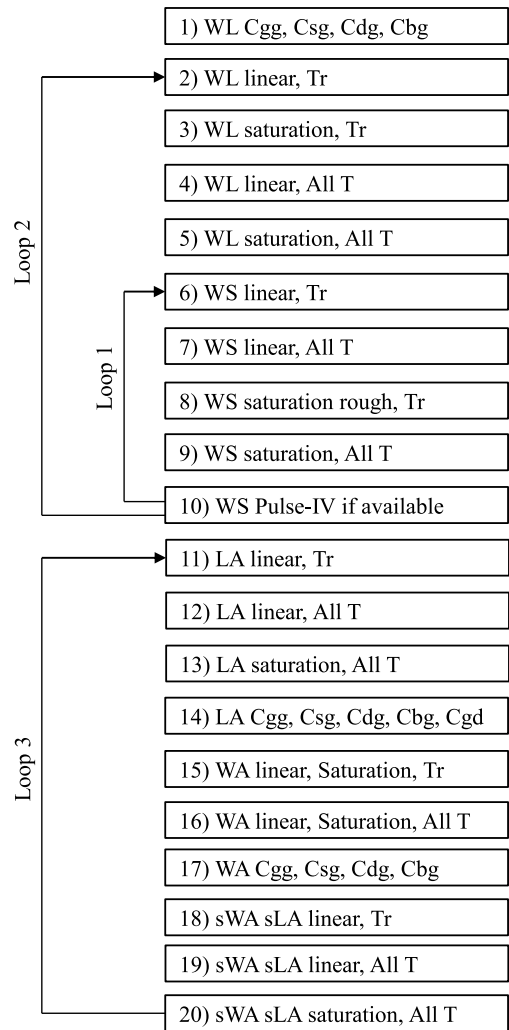


FIGURE 4. Extraction flow.

- CV data for WL, WS, NL, NS devices at T_r
 - *cxg*: $C_{xg}(V_{gs})$ at $V_{ds} = V_{bs} = 0$
 - *cgd*: $C_{gd}(V_{ds})$ at $V_{gs} = V_{bs} = 0$
- (optional) *s*-parameter data for the WS device at T_r
 - *y22*: $y_{22}(f)$ from 10 kHz to 10 MHz, $V_{gs} = V_{gs,max}/2$, $V_{ds} = V_{ds,max}/2$, $V_{bs} = 0$
 - *cxg_spar*: $C_{xg}(V_{gs})$ from *s*-parameters, for V_{gs} from $-V_{gs,max}$ to $+V_{gs,max}$, several values of V_{ds} from 0 to $V_{ds,max}/2$, $V_{bs} = 0$, $f = 2$ GHz
- (optional) pulsed IV data for the WS device at T_r
 - *idvd_pulse*: $I_d(V_{ds})$ and $I_b(V_{ds})$ for several V_{gs} in strong inversion, $V_{bs} = 0$

To avoid damaging devices, the highest V_{ds} for *idvg_sat* and *idvd* data may be limited to $V_{ds,max}/2$. Structures for capacitance and *s*-parameter data should have a sufficient number of gates N_g to enable reliable measurement.

IV. EXTRACTION FLOW

Fig. 4 shows the steps in our flow, which are detailed below. Unless otherwise stated, the data are for a 45V n-LDMOS

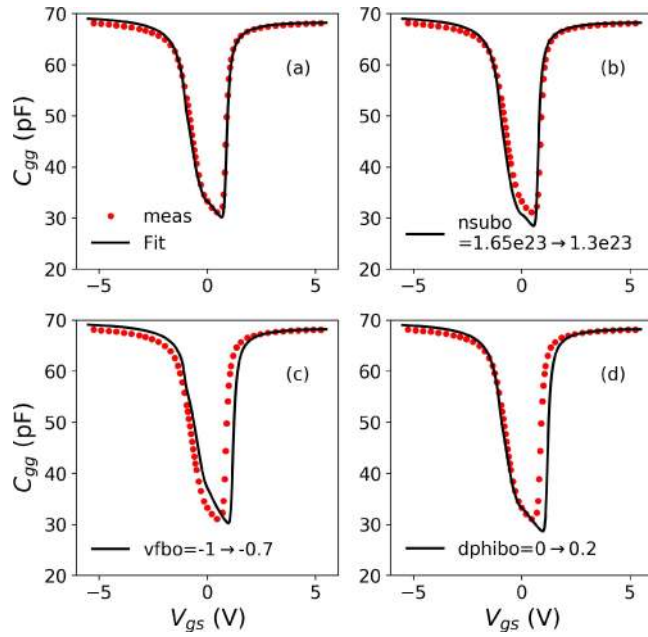


FIGURE 5. C_{gg} of a WL transistor, $W/L/N_g = 25 \mu\text{m}/10 \mu\text{m}/112$, $V_{ds} = V_{bs} = 0 \text{ V}$.

transistor in a 90nm BCD technology at $T = T_r = 25 \text{ }^\circ\text{C}$, measured data are plotted as symbols, and PSPHV model results are plotted as lines. If devices have the bulk and source tied, omit parameters and steps that require V_{sb} and I_b data.

Following the PSP parameter naming convention, paramo is the geometry independent part for param (WL device); paraml models the L dependence (WS device); paramw models the W dependence (NL); and paramlw models the area dependence (coupled L and W dependence, NS device). Refer to the Appendix for the meaning of each parameter.

Selection and technology parameters:

- set type to +1/−1 for n/p-type transistors, respectively
- set tr and trj to the reference temperature
- if the device has no halo implant, set lpck = 0
- set lgdov based on the device cross-section and layout
- for devices with a second gate-drain overlap region, set lgdov2 and toxovd2o from technology data

JFETIDG has several ways to define and calculate the sheet resistance of the drift region, see [3, Fig. 4]; we recommend specifying rsh0.

Step 1: device: WL, data: cgg, temperature: T_r .

Extract the gate oxide thickness toxo by fitting the capacitance data for $V_{gs} = \pm V_{gs,max}$. Set toxovo = toxovdo = toxo. The bulk doping nsubo then determines the minimum C_{gg} , see Fig. 5(b). The flat band voltage vfb0 shifts the whole C_{gg} curve horizontally, as Fig. 5(c) shows, and should be used to fit the data in depletion. The offset of the bulk potential ϕ_B , dphibo, only affects C_{gg} in inversion as Fig. 5(d) shows. Fig. 5(a) shows the final fit. If the influence of poly depletion is apparent include npo.

Step 2: device: WL, data: idvg_lin, temperature: T_r .

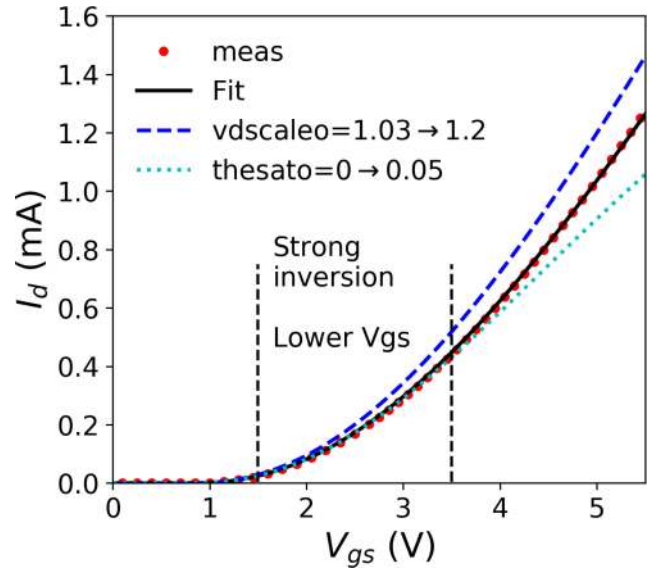


FIGURE 6. $I_d(V_{gs})$ of a WL transistor, $W/L/N_g = 25 \mu\text{m}/25 \mu\text{m}/2$, $V_{ds}=28 \text{ V}$ and $V_{bs}=0$.

Extract nsubo, dphibo, and the interface charge factor cto to fit the data in weak inversion; if gradual channel turn on is apparent include the gate dependence of interface charge ctgo, see [1, Fig. 6]. For the data in strong inversion, extract mobility related parameters uo, mueo, themuo and, at high V_{bs} , the non-universality parameter xcoro.

Step 3: device: WL, data: idvg_sat, temperature: T_r .

Extract the velocity saturation parameters thesato and thesatgo at $V_{bs} = 0$, thesatbo at high V_{bs} . If the model underestimates I_d even with thesato = 0 use the V_{di} scaling parameter vdscaleo. Fig. 6 shows the effect of vdscaleo and thesato. vdscaleo affects strong inversion for all V_{gs} , thesato mainly impacts the higher V_{gs} region. Therefore, use vdscaleo to fit strong inversion data at lower V_{gs} . This V_{ds} scaling technique [16] is an important feature of PSPHV, not available in PSP, and significantly improves modeling of short channel devices where NULD is significant. A similar technique is also used in the BSIM-BULK model [17].

Extract the smoothing parameter aro of the new $C^\infty V_{dsat}$ clamping function in PSPHV [18] by fitting the nonsaturation to saturation transition region.

Extract the avalanche current parameter a1o, a2o, a3o and a3cvd1; a3cvdo to fit I_b . Fig. 11(b) shows the influence of a3cvd1; a3cvdo has similar effect.

Step 4: device: WL, data: idvg_lin, temperature: all.

Extract the temperature dependence parameters stvfb0, stbeto, stmueo, and stthemueo at $V_{bs} = 0$. From the data at high V_{bs} extract stxcoro.

Step 5: device: WL, data: idvg_sat, temperature: all.

Extract stthesato and, if vdscaleo is used, stvdscaleo.

The temperature dependence parameters for the WL device, which is not significantly affected by SHE, are

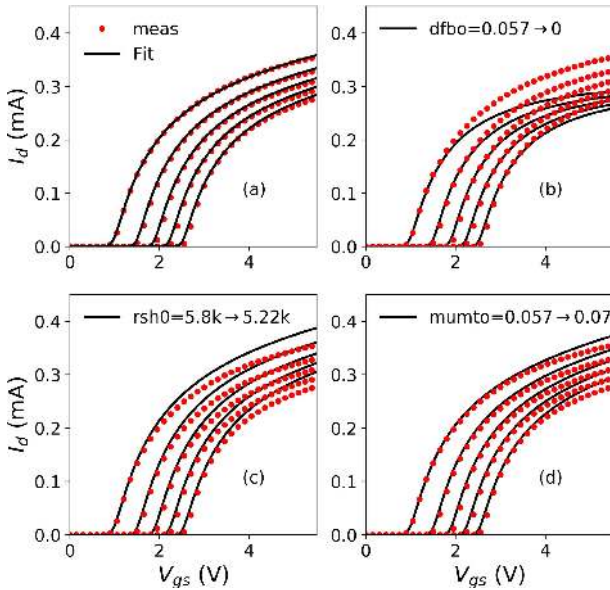


FIGURE 7. $I_d(V_{gs})$ of a WS transistor, $W/L/N_g = 25 \mu\text{m}/1 \mu\text{m}/2$, $V_{bs} = 0, -1.25, -2.5, -3.75, -5 \text{ V}$, $V_{ds} = 0.1 \text{ V}$.

extracted before fitting the WS device, to ensure those parameters for the long channel device are correct.

Step 6: device: WS, data: idvg_lin, temperature: T_r .

Extract ct1 , dphib1 , and foll to fit I_d in weak inversion. The intrinsic series resistance rsw1 can be set to zero, its impact is small and can be subsumed into the drift resistance. Extract the drift region bottom gate depletion parameter dfbo to match the spacing between the curves for different V_{bs} at $V_{gs,max}$, see Fig. 7(b) for the impact of dfbo . Roughly extract the effective channel length offset parameter lvaro to fit the peak g_m . Figs. 7(c) and 7(d) show how rsh0 and mumto affect fitting; rsh0 has an influence over a wide range of V_{gs} whereas mumto affects fitting at high V_{gs} . By tuning lvaro , rsh0 , and mumto , the nonsaturation data can be fitted well, as Fig. 7(a) shows. Fig. 8(a) shows g_m at different V_{bs} .

Step 7: device: WS, data: idvg_lin, temperature: all.

Extract the temperature dependence of the intrinsic MOS transistor channel mobility stbet1 from peak g_m . Extract the temperature dependence of the drift region mobility, and hence resistance, tc1o and tc2o from the high V_{gs} region. Coupled through SHE, these parameters affect the saturation characteristics at T_r , see Fig. 9. This is why the temperature dependence of the nonsaturation characteristics must be extracted before fitting the saturation characteristics at T_r .

Note that tc1o and tc2o directly affect the temperature dependence of ecrit through $E_{crit} = V_{sat}/\mu$. This coupling complicates extraction but is crucial for self-consistent modeling of output characteristics with and without SHE, as noted in [1].

Step 8: device: WS, data: idvg_sat and idvd, temperature: T_r .

Here, the device characteristics are impacted by many physical effects such as the velocity saturation of the intrinsic

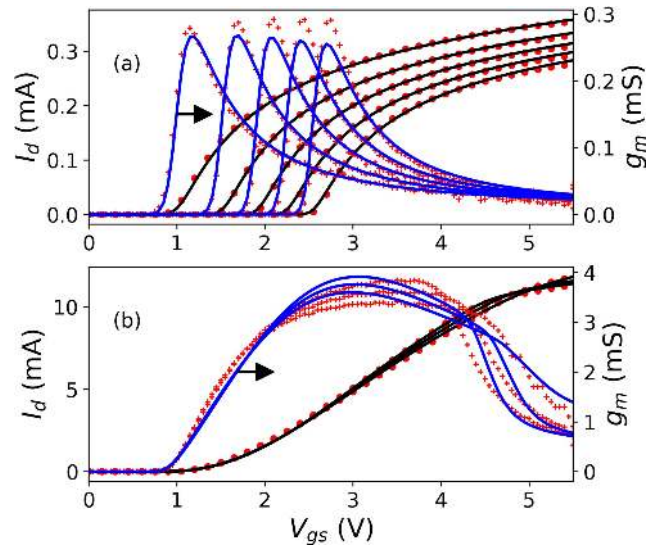


FIGURE 8. (a) $I_d(V_{gs})$ and $g_m(V_{gs})$, same transistor and biases as Fig. 7. (b) $I_d(V_{gs})$ and $g_m(V_{gs})$ for the same transistor, $V_{ds} = 12, 20, 28 \text{ V}$, $V_{bs} = 0 \text{ V}$.

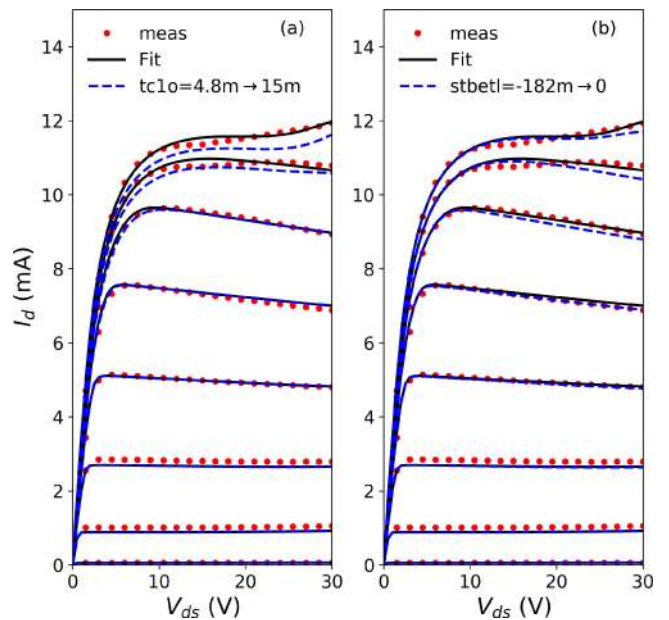


FIGURE 9. $I_d(V_{ds})$ of the WS transistor as Fig. 7 at different V_{gs} . The temperature coefficients tc1o (a) and stbet1 (b), extracted from idvg_lin data, affect the saturation characteristics at T_r .

MOS, the quasi-saturation of the drift region, and the impact ionization in both the intrinsic MOS and the drift region. This is a complicated part of LDMOS extraction: fitting at T_r , in the presence of SHE, depends on temperature coefficients of parameters that have influence in saturation, however from the previous step we only have, so far, temperature coefficients for the parameters dominant at low V_{ds} . This step is a first rough extraction, that is refined in the next step.

8.1 Extract the DIBL parameter cfl to fit idvg_sat data in weak inversion.

8.2 The thermal conductance in PSPHV scales as

$$g_{th} = g_{tho} + g_{thi}L + g_{thw}W + g_{tha}LW. \quad (2)$$

This points to “extract g_{tha} from the WL device.” However, SHE is weak for that device, to first order SHE decreases as $1/L^2$, so that is not possible. This leaves two practical options: extract g_{tha} from the WS device; or use TCAD to develop a scaling equation based on thermal simulation, then extract a scale factor to calibrate the TCAD-based model so the PSPHV results match silicon data. It is possible to determine g_{th} for devices that exhibit negative g_o . However, in practice g_{th} scaling can be significantly more complex than (2), especially when multiple device fingers are included. Because of the high currents involved, it can be difficult to measure $I_d(V_{ds})$ at moderate to high V_{ds} for short multi-finger devices. For this reason we prefer to use TCAD to develop a scalable g_{th} model, including multi-finger devices.

g_{th} determines the (negative) slope in output characteristics at high V_{gs} . Fig. 10(a) compares $idvd$ data with and without SHE. The scale factor for the TCAD based g_{th} scaling model is extracted to fit the slope at moderate V_{gs} biases, see the ellipse in Fig. 10(a).

8.3 Use the $idvg_{sat}$ data before the onset of quasi-saturation to extract $thesat1$ and $vdscale1$; their effect is the same as for the associated geometry independent parameters $thesato$ and $vdscaleo$, respectively, see Fig. 6. Then use $idvd$ data to extract the drift region velocity saturation parameters $ecrito$ and $ecorno$ for quasi-saturation effect; Fig. 10(b) and 10(c) show the effect of these parameters, respectively. The V_{dsat} smoothing parameter for short devices, $ar1$, can also be used to tune the transition region, in concert with $ecorno$.

At high V_{gs} and moderate V_{ds} , the parameter for the Early effect in the drift region $clm11$ may be needed. Fig. 10(d), compared to Fig. 10(a), shows how $clm11$ affects the output conductance. Do not make $clm11$ too large otherwise it leads to overprediction of I_d in comparison to pulsed $I_d(V_{ds})$ data when SHE is turned off.

At this point, do not fit the high V_{gs} and high V_{ds} region because the avalanche current parameters have not been extracted.

8.4 To extract parameters for the avalanche current, note that it has components both from the intrinsic MOS transistor, at lower V_{gs} , and from the Kirk effect in the drift region, at higher V_{gs} , see Fig. 11(a). If you have to invoke V_{di} clamping, see Section V, set $swvdimp = 1$ to enable better avalanche current modeling.

Extract $a11$, $a31$, and $a3cvd1$ to fit I_b at lower V_{gs} , Fig. 11(b) shows the effect of $a3cvd1$. Extract Kirk effect related parameters $alphabo$, $beta$, mhc , and jhc to fit I_b at higher V_{gs} . $alphabo$ controls the magnitude of the avalanche current in the drift region, Fig. 11(c) shows the effect of setting it to zero (the increase in I_b at high V_{gs} in that plot is the result of using $V(d,s)$ instead of $V(di,s)$ to calculate the avalanche current, from $swvdimp = 1$). $beta$ controls the spacing between the Kirk effect curves.

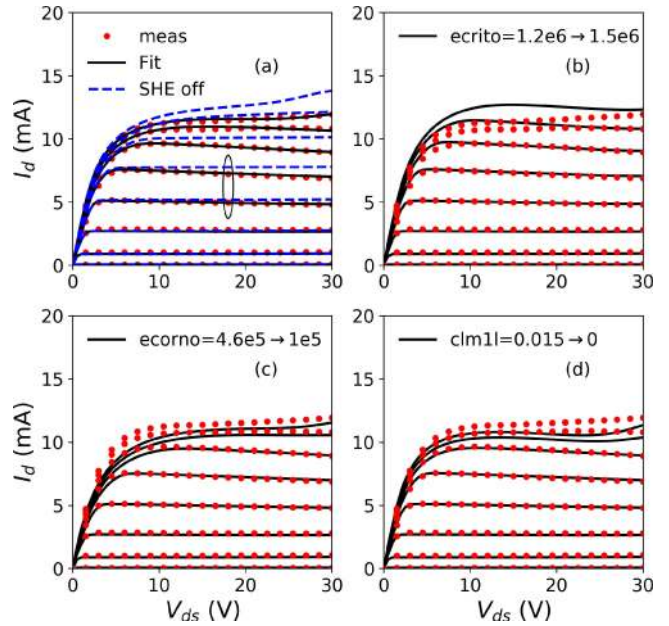


FIGURE 10. $I_d(V_{ds})$ of the WS transistor of Fig. 7 at different V_{gs} , $V_{bs} = 0$.

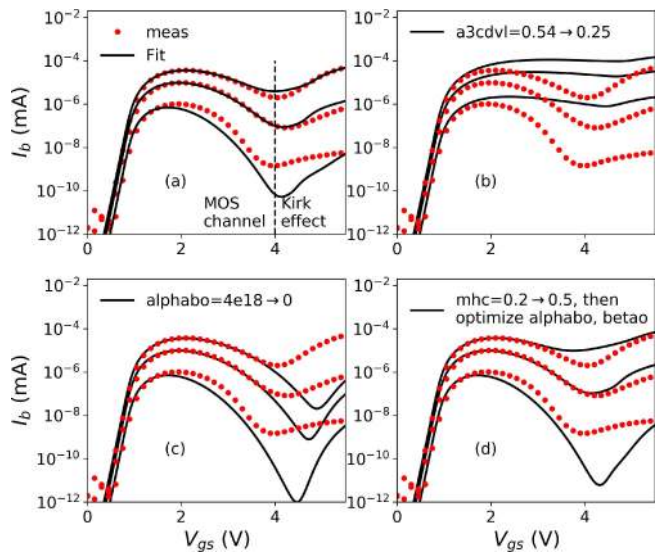


FIGURE 11. $I_b(V_{gs})$ of the WS transistor of Fig. 7 at different V_{ds} , $V_{bs} = 0$.

mhc reflects the influence of the doping profile of the drift region, increasing it lowers I_b at low V_{ds} , see Fig. 11(d).

Step 9: device: WS, data: $idvd$ and $y22$, temperature: all.

First, extract $tegth$, the temperature coefficient of g_{th} , to fit g_o at all temperatures. Then extract $xvsato$, the temperature dependence of velocity saturation in the drift region, see Fig. 12(b). These temperature dependence parameters also affect fitting at T_r because of SHE, which is why WS saturation parameters need to be fitted to data from all temperatures.

Next, extract $sta2o$ and $xbeta$ for the temperature dependence of avalanche current. Extract the drain expansion parameters $mumi1o$ and $mumi2o$ (Section VI gives

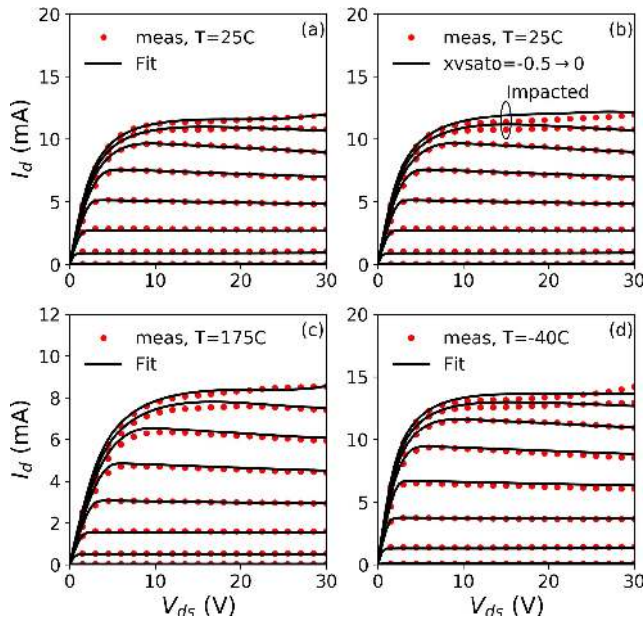


FIGURE 12. $I_d(V_{ds})$ of the WS transistor of Fig. 7 at different V_{gs} , (a), (c), and (d) show fitting over temperature, (b) shows the impact of $xvssato$.

further details), and optimize $ecrito$, $gtha$, $tegth$, and $xvssato$ to fit $idvd$ data over all temperatures. Figs. 12(a), 12(c), and 12(d) show results after these steps at 25, 175, and -40°C , respectively. Excellent fitting has been achieved. Fig. 8(b) shows that g_m at different V_{ds} is also modeled well.

To extract thermal capacitance parameters, the best approach is to develop a scaling model using TCAD, then use a scale factor to fit that model to $\Re(y_{22})$ versus frequency, see Fig. 13. The thermal capacitance c_{th} adjusts the frequency at which g_o transitions from being affected, to not being affected, by SHE.

If y_{22} data are not available, measurements from a variety of devices show that thermal time constants for integrated devices vary from about 0.1 to 10.0 μs , with 1 μs being a typical value. So, set the scaling and value such that $c_{th}/g_{th} = 10^{-6}$ s.

Step 10: device: WS, data: $idvd_pulse$, temperature: T_r .

Because pulsed IV data remove the SHE they are useful to verify, and refine if necessary, the accuracy of modeling of g_o of the intrinsic transistor. If I_d in saturation in the pulsed IV data are not modeled accurately, adjust the channel length modulation parameter $clm11$ to improve the fit. See [1, Fig. 14] for an example. $clm11$ changes the slope of output curves in the quasi-saturation region. Note that pulsed IV and DC data cannot be fitted simultaneously; they are typically measured on separate structures, so local variation between devices and differences in series resistance between the structures affect the results. Factor those differences in when adjusting to fit the pulsed IV data.

Loop 1: To improve fitting in both nonsaturation and saturation for the WS device, repeat steps 6 through 10, see Fig. 4.

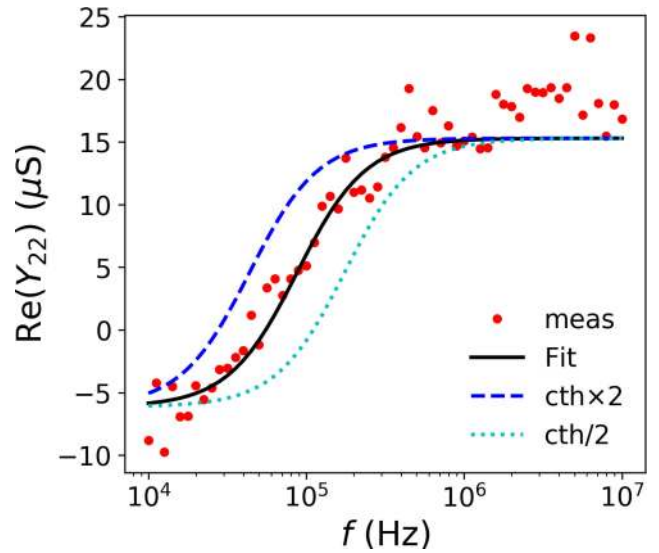


FIGURE 13. $\Re(Y_{22})$ vs. f of a WS 90V p-LDMOS transistor, $V_{gs} = 3.5$ V, $V_{ds} = 35$ V, $T = 27^\circ\text{C}$.

Loop 2: Repeat steps 1 through 10, see Fig. 4, to fine tune parameters for the WL device.

Step 11: devices: LA, data: $idvg_lin$, temperature: T_r .

This step determines “shape” parameters for the length dependence of wide devices in nonsaturation. Optimize uo , $lvaro$, and $lvar1$ to fit peak g_m . (The other option is to use $fbet1$ and $lp1$ instead of $lvar1$.) Optimize cto , $ctgo$, ctl , and $ctlexp$ to fit subthreshold slope. Optimize $nsubo$, $vfbo$, $dphibo$, $fol1$, $fol2$, $vfb1$, $dphib1$, and for devices with halo implants $lpck$ and $npck$, to fit threshold voltage. Optimize $mueo$, $themuo$, $xcoro$, $rsh0$, $mumto$, and $dfbo$ to fit data at high V_{gs} .

Step 12: devices: LA, data: $idvg_lin$, temperature: all.

This step determines “shape” parameters for temperature dependence over length of wide devices in nonsaturation. Optimize the temperature dependence parameters $stvfbo$, $stbeto$, $stmueo$, $stthemueo$, $stxcoro$, $stvfbl$, $stbet1$, $tc1o$, and $tc2o$ to fit the $idvg_lin$ data over temperature.

Step 13: devices: LA, data: $idvg_sat$ and $idvd$, temperature: all.

This step determines “shape” parameters for the length and temperature dependence of wide devices in saturation. Optimize cfl , and $cfllexp$ to model DIBL in the $idvg_sat$ data. Using both $idvg_sat$ and $idvd$ data, optimize $thesato$, $thesat1$, $thesatlexp$, $thesatgo$, $vdscaleo$, $vdscale1$, and $vdscalele$ to fit I_d before the onset of quasi-saturation onset, optimize aro , arl , $arlexp$, and $ecorno$ to fit the region around the transition to saturation, and optimize $ecrito$, $gtha$, $tegth$, and $xvssato$ to fit the quasi-saturation region.

Step 14: devices: WS, data: cgg , csg , and cdg , temperature: T_r .

This step fits source and drain overlap capacitances and the channel length offset for charge to fit total gate capacitance.

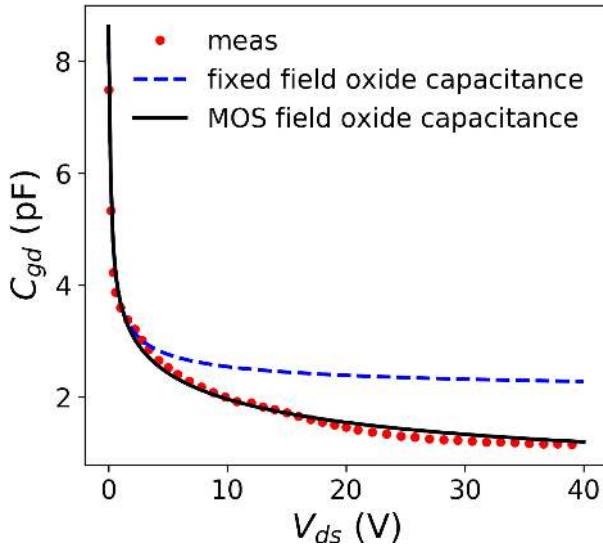


FIGURE 14. C_{gd} vs. V_{ds} for a WS transistor, $W/L/N_g = 25 \mu\text{m}/1 \mu\text{m}/280$, $V_{gs} = 0$, $f = 1 \text{ MHz}$, $T = 25^\circ\text{C}$.

Extract lov , $vfbv$, $novo$, and $cfrw$ to fit csg , $xlgdovq$, $novdo$, and $vfbvd$ to fit cdg , and dlq to fit cgg . The field plate can be modeled as a bias independent capacitor or as a MOS capacitor through $lgdov2$ and $toxovd2o$. As Fig. 14 shows, the latter greatly improves C_{gd} modeling.

Step 15: devices: WA, data: $idvg_lin$ and $idvg_sat$, temperature: T_r .

This step determines “shape” parameters for width dependence of long devices in both nonsaturation and saturation. From the $idvg_lin$ data, extract the effective channel width offset parameters $wvaro$ and $wvarw$ to fit peak g_m (the other option is to use $fbetw1$ and $betw1$ instead of $wvarw$), extract $dphibw$ to fit threshold voltage, and extract $muew$ to fit I_d at high V_{gs} . From the $idvg_sat$ data, extract $thesatw$ and $vdscalew$.

Step 16: devices: WA, data: $idvg_lin$ and $idvg_sat$, temperature: all.

This step determines “shape” parameters for temperature dependence over width of long devices in both nonsaturation and saturation. Extract $stvfwb$ and $stbetw$ to fit the $idvg_lin$ data over temperature. Extract $stthesatw$ and $stvdscalew$ to fit the $idvg_sat$ data over temperature.

Step 17: devices: WA, data: cgg and cbg , temperature: T_r .

This step fits gate-bulk overlap capacitance and the channel width offset for charge to fit total gate capacitance. Extract $cgbovl$ to fit cbg , extract dwq to fit cgg .

Step 18: devices: sLA and sWA, data: $idvg_lin$, temperature: T_r .

This step determines “shape” parameters for coupled length and width interactions in nonsaturation. Extract $lvarw$ to fit peak g_m . Extract $vfbw$ and $dphibw$ to fit threshold voltage. Extract $ctlw$ to fit subthreshold slope. Extract xw to fit I_d at high V_{gs} . Extract $dfbw$ to fit the V_{bs} dependence at high V_{gs} .

Step 19: devices: sLA and sWA, data: $idvg_lin$, temperature: all.

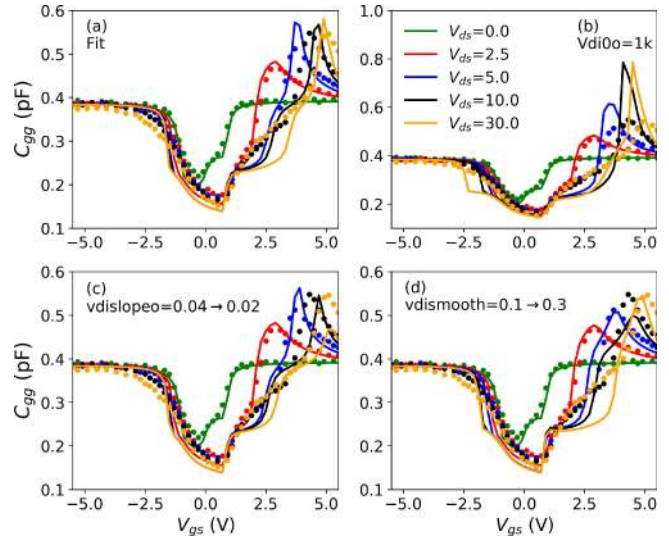


FIGURE 15. C_{gg} vs. V_{gs} for a WS transistor, $W/L/N_g = 10 \mu\text{m}/1 \mu\text{m}/8$, $f = 2 \text{ GHz}$, $T = 25^\circ\text{C}$.

This step fits the temperature parameters for coupled length and width interactions in nonsaturation. Extract $stvfblw$ to fit threshold voltage, and $stbetlw$, $tc1w$, and $tc2w$ to fit I_d at high V_{gs} .

Step 20: devices: sLA and sWA, data: $idvg_sat$ and $idvd$, temperature: all.

This step fits coupled length and width interactions in saturation. Extract $thesatlw$, $vdscalelw$, and $ecritw$ to fit both sets of data.

Loop 3: To improve fitting in both nonsaturation and saturation, over bias, geometry, and temperature, repeat steps 11 through 20, see Fig. 4.

V. V_{di} CLAMPING AND ITS EFFECT ON C_{GD} AND Q_G

Figs. 15(a) and 15(b) show PSPHV modeling of gate capacitance with and without V_{di} clamping, respectively. The spikes at high V_{ds} visible in 15(b) are eliminated when V_{di} clamping is used, see 15(a). These spikes typically only occur for high voltage transistors; for low voltage transistors and transistors that do not exhibit such spikes in capacitance do not turn on V_{di} clamping (there is a computational cost associated with the clamping).

If the capacitances do exhibit spikes, set $swvdiclamp = 1$ and the clamping voltage parameter $vdi0o$ to a starting value of $V_{gs,max}$. Note that data from s -parameter test structures are needed to extract V_{di} clamping parameters.

The parameter $vdislopeo$ adjusts the V_{ds} dependence of the clamped V_{di} , see Fig. 15(c). $vdismooth$ smooths the clamping, as Fig. 15(d) shows.

Adjust $vdi0o$, $vdismooth$, $vdislopeo$, and $vdislopego$ (the V_{gs} dependence of the clamped V_{di}) to fit the measured C_{gg} data.

Fig. 16 shows the impact of V_{di} clamping on $C_{gd}(V_{ds})$, where the field plate is modeled as a bias independent plate capacitor. The modeled C_{gd} drops at the V_{di} clamping voltage because V_{ds} can no longer change the intrinsic transistor C_{gd}

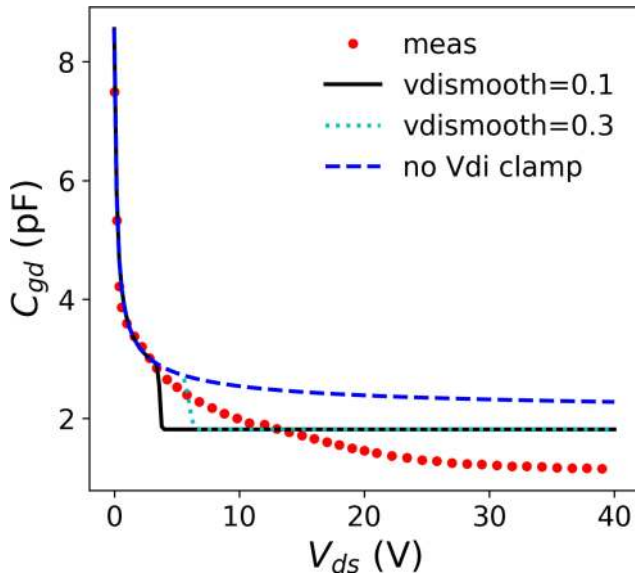


FIGURE 16. C_{gd} vs. V_{ds} , same transistor as Fig. 14, $V_{gs} = 0$, $f = 1$ MHz, $T = 25$ °C.

after V_{di} is clamped. In reality, the clamping occurs gradually, through the bias dependence of the lateral depletion in the gate-drain overlap region; this phenomena is not modeled physically in PSPHV. A larger $vdis\ smooth$ helps reduce the abruptness of the drop, see Fig. 16. For this device, the use of $lgdov2$ readily gives a good fit, as Fig. 14 shows. However, for very high voltage devices, the drop in C_{gd} can happen even if a MOS, rather than fixed, capacitor is used for the second gate-drain overlap region. For such devices V_{di} clamping gives more accurate modeling of the total charge $\int C_{gd} dV_d$, and therefore more accurate modeling of switching losses.

Fig. 17 shows simulated gate charging characteristics, V_{gs} vs. Q_g . V_{di} clamping reduces the Q_g at which the transistor turns on, as expected. However, the clamping introduces a small kink at low V_{gs} , see the inset in Fig. 17. The kink becomes worse as $vdis\ smooth$ increases, so keep $vdis\ smooth \leq 0.3$.

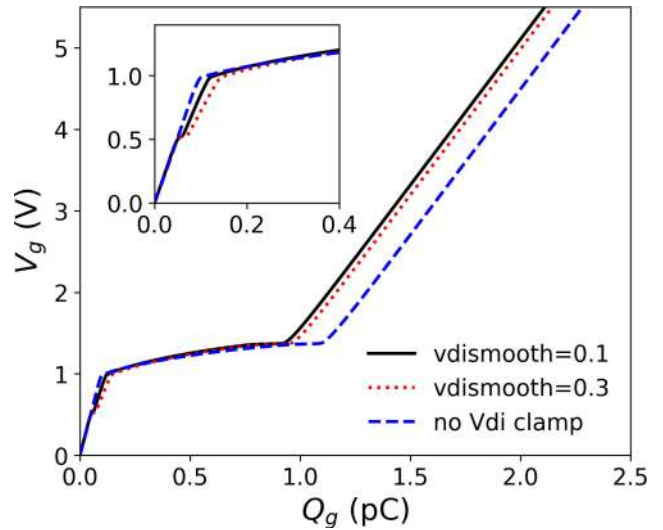


FIGURE 17. V_{gs} vs. Q_g for a WS transistor, $W/L/N_g = 30 \mu\text{m}/1 \mu\text{m}/2$, $T = 25$ °C.

VI. EXTRACTION FOR THE DRAIN EXPANSION EFFECT

PSPHV models the drain expansion effect [19] through modulation of the conductivity of the drift region by impact ionization. Fig. 18(a) shows $I_d(V_{ds})$ for a transistor with pronounced drain expansion; clearly, PSPHV can model this effect well. The body and source are shorted for this device, I_b is not directly available, so we fit I_d where it has a significant component from impact ionization.

Modeling the drain expansion effect requires simultaneous fitting of avalanche current and conductivity modulation by that current.

First, extract the intrinsic transistor avalanche parameters $a1o$ and $a2o$ to fit $I_d(V_{ds})$ at low V_{gs} and high V_{ds} (the avalanche current there is dominated by the intrinsic transistor), and to fit the data at moderate V_{gs} , where the Kirk effect

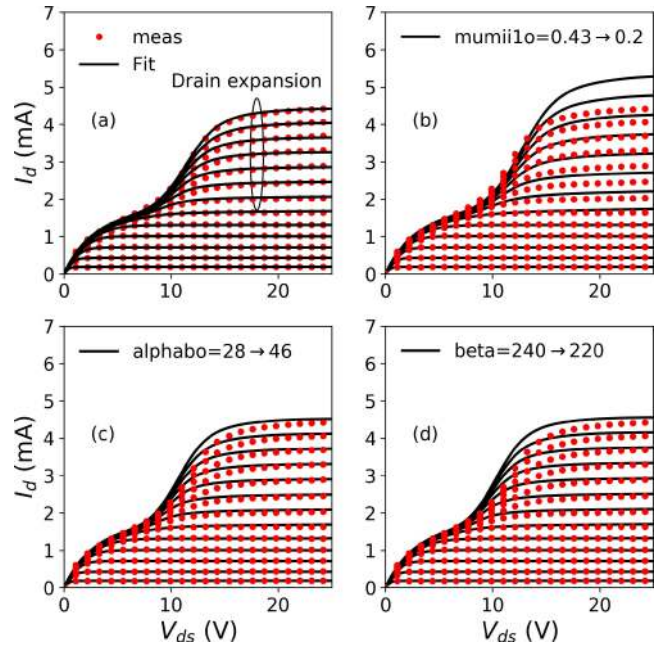


FIGURE 18. $I_d(V_{ds})$ for a 65V power n-LDMOS transistor that exhibits strong expansion effect. Bottom to top: $V_{gs} = 2$ to 8 V by 0.5 V, $T = 27$ °C.

in the drift region becomes significant, roughly initialize beta and alphabo.

Second, the parameter $mumi1o$, which models drift region conductivity modulation due to avalanche current, determines the point at which the expansion effect starts, see Fig. 18(b). Extract $mumi1o$ to align this onset point between PSPHV and the data.

Third, extract $alphabo$ to fit I_d at high V_{ds} . This parameter affects the whole expansion region, see Fig. 18(c). Tune $vdscaleo$, $thesato$, and $thesatgo$ as well to fit I_d over all V_{ds} .

Finally, check the slope of I_d expansion just above the onset of the expansion effect. If the slope in the modeled I_d

is too small, first reduce beta and re-optimize. Fig. 18(d) shows the effect of beta on slope of the expansion effect. If the fitting is still not good enough, also include the second order conductivity modulation parameter `mumii2o`.

VII. CONCLUSION

We have described a global scaling, self-heating effect aware, large signal parameter extraction method for PSPHV. The parameters important for each extraction step are detailed, and graphical illustrations of the effect of key parameters for effects unique to PSP are provided, these include: drain voltage scaling; the Kirk effect in the drift region; internal drain voltage clamping to suppress spikes in capacitance; and the drain expansion effect. The extraction flow is verified against experimental DC and CV data from -40°C to 175°C . Fully scalable and accurate models have been extracted with this method.

APPENDIX

Below is the description of the used model parameters in alphabetical order. `paramo/l/w/lw` stands for the geometry independent parameter `paramo` and the geometry dependence parameters `paraml`, `paramw`, and `paramlw`. II means impact ionization, DR means drift region.

| | | | |
|-----------------------------|---|----------------------------|--|
| <code>a1o/l</code> | channel II pre-factor | <code>ecrito/w</code> | velocity saturation critical field |
| <code>a2o</code> | channel II exponent | <code>fbet1/w</code> | relative mobility decrease due to first lateral profile |
| <code>a3cvdo/l</code> | drain voltage dependence of <code>a3</code> | <code>fol1</code> | first length dependence coefficient for short channel body effect |
| <code>a3o/l</code> | saturation-voltage dependence of II | <code>fol2</code> | second length dependence coefficient for short channel body effect |
| <code>alphabo</code> | DR bottom gate II magnitude | <code>gtho/l/w/a</code> | thermal conductance |
| <code>aro/l</code> | saturation transition smoothing | <code>jhc</code> | threshold current for DR impact ionization Kirk effect |
| <code>beta</code> | DR II current exponent for both gates | <code>lov</code> | gate-source overlap length for capacitance |
| <code>betw1</code> | first higher-order width scaling coefficient of gain factor | <code>lpck</code> | characteristics length of lateral doping profile |
| <code>cf1</code> | length dependence of DIBL | <code>lp1</code> | mobility-related characteristic length of first lateral profile |
| <code>cflexp</code> | exponent for length dependence of DIBL | <code>lvaro/l/w</code> | difference between actual and programmed gate length |
| <code>cgbovl</code> | gate-bulk overlap capacitance per L_{EN} | <code>mhc</code> | power for DR II current |
| <code>clm1l</code> | <code>clm1</code> length dependence coefficient | <code>mueo/w</code> | mobility reduction coefficient |
| <code>ctgo</code> | gate voltage dependence of interface states factor | <code>mumii1o</code> | 1st order DR II modulation effect |
| <code>ctho/l/w/a</code> | thermal capacitance | <code>mumii2o</code> | 2nd order DR II modulation effect |
| <code>ctlexp</code> | exponent for length dependence of interface states factor | <code>mumto</code> | DR top gate modulation effect on mobility |
| <code>cto/l/w/lw</code> | interface states factor | <code>novdo</code> | drain overlap region effective doping |
| <code>dfbo/w</code> | DR bottom gate depletion factor | <code>novo</code> | source overlap region effective doping |
| <code>dfto</code> | DR top gate depletion factor | <code>npck</code> | pocket doping level |
| <code>dlq</code> | effective channel length reduction for capacitance | <code>npo</code> | gate poly-silicon doping |
| <code>dphibo /l/w/lw</code> | offset of ϕ_b | <code>nsubo</code> | bulk doping |
| <code>dwq</code> | effective channel width reduction for capacitance | <code>psirto</code> | twice the built-in potential of the DR top gate |
| <code>ecorno</code> | velocity saturation corner field | <code>rsh0</code> | DR zero-bias sheet resistance |
| | | <code>rsw1</code> | Series resistance |
| | | <code>sta2o</code> | temperature dependence of <code>a2</code> |
| | | <code>stbeto/l/w</code> | temperature dependence of gain factor |
| | | <code>stmueo</code> | temperature dependence of <code>mue</code> |
| | | <code>stthemuo</code> | temperature dependence of <code>themu</code> |
| | | <code>stthesato/w</code> | temperature dependence of <code>thesat</code> |
| | | <code>stvdscaleo/w</code> | temperature dependence of <code>stvdscale</code> |
| | | <code>stvfbo/l/w/lw</code> | temperature dependence of <code>vfb</code> |
| | | <code>stxcoro</code> | temperature dependence of <code>xcor</code> |
| | | <code>tc1o/w</code> | first order temperature coefficient for DR resistance |
| | | <code>tc2o/w</code> | second order temperature coefficient for DR resistance |
| | | <code>tegth</code> | thermal conductance temperature exponent |
| | | <code>themuo</code> | mobility reduction exponent |

| | |
|------------------|--|
| thesatbo | bulk voltage dependence of velocity saturation |
| thesatgo | gate voltage dependence of velocity saturation |
| thesatlexp | exponent for length dependence of thesat |
| thesato/l | temperature dependence of velocity saturation |
| toxo | gate oxide thickness |
| toxovd2o | oxide thickness for second gate-drain overlap |
| toxovdo | oxide thickness thickness for gate-drain overlap |
| toxovo | oxide thickness thickness for gate-source overlap |
| uo | zero-field mobility |
| vdi0o/l | clamping voltage for V_{di} |
| vdislopeo | drain voltage dependence of V_{di} clamping |
| vdislopgo | gate voltage dependence of V_{di} clamping |
| vdismooth | smoothing factor for V_{di} clamping |
| vdscalebo/l/w/lw | bulk voltage dependence of V_{ds} scaling |
| vdscalele | exponent for length dependence of V_{ds} scaling |
| vdscaleo/l/w/lw | V_{ds} scaling factor for NULD |
| vfbo/l/w/lw | flat-band voltage |
| vfbov | flat-band voltage for gate-source overlap |
| vfbovd | flat-band voltage for gate-drain overlap |
| wvaro/w | difference between actual and programmed field-oxide opening |
| xbeta | temperature exponent of DR II parameter beta |
| xcoro | non-universality parameter |
| xlgdovq | length offset for gate-drain overlap capacitance |
| xvsato | temperature exponent of DR saturated velocity |
| xw | DR width offset. |

REFERENCES

- [1] K. Xia, C. C. McAndrew, R. van Langevelde, G. D. J. Smit, and A. J. Scholten, "PSPHV: A surface-potential-based model for ldmos transistors," *IEEE Trans. Electron Devices*, vol. 66, no. 12, pp. 5246–5253, Dec. 2019, doi: [10.1109/TED.2019.2945832](https://doi.org/10.1109/TED.2019.2945832).
- [2] *PSP 103.6 Model Manual*. Accessed: Sep. 2019. [Online]. Available: http://www.cea.fr/cea-tech/leti/pspsupport/Documents/psp103p6_summary.pdf.
- [3] K. Xia and C. C. McAndrew, "JFETIDG: A compact model for independent dual-gate JFETs with junction or MOS gates," *IEEE Trans. Electron Devices*, vol. 65, no. 2, pp. 747–755, Feb. 2018, doi: [10.1109/TED.2017.2786043](https://doi.org/10.1109/TED.2017.2786043).
- [4] A. J. Scholten, G. D. J. Smit, R. van Langevelde, and D. B. M. Klaassen, "The JUNCAP2 model for junction diodes," in *Compact Modeling: Principles, Techniques and Applications*. G. Gildenblat, Ed. New York, NY, USA: Springer, 2010, ch. 10, pp. 299–326, doi: [10.1007/978-90-481-8614-3](https://doi.org/10.1007/978-90-481-8614-3).
- [5] *PSPHV LDMOS 1.0.3*. Accessed: Apr. 2020. [Online]. Available: <https://nanohub.org/projects/psphvldmos>
- [6] W. Yao, G. Gildenblat, C. C. McAndrew, and A. Cassagnes, "SP-HV: A scalable surface-potential-based compact model for LDMOS transistors," *IEEE Trans. Electron Devices*, vol. 59, no. 3, pp. 542–550, Mar. 2012, doi: [10.1109/TED.2011.2177092](https://doi.org/10.1109/TED.2011.2177092).
- [7] H. Agarwal *et al.*, "BSIM-HV: High-voltage MOSFET model including quasi-saturation and self-heating effect," *IEEE Trans. Electron Devices*, vol. 66, no. 10, pp. 4258–4263, Oct. 2019, doi: [10.1109/TED.2019.2933611](https://doi.org/10.1109/TED.2019.2933611).
- [8] H. J. Mattausch, M. Miyake, T. Iizuka, H. Kikuchihara, and M. M. Mattausch, "The second-generation of HiSIM_HV compact models for high-voltage MOSFETs," *IEEE Trans. Electron Devices*, vol. 60, no. 2, pp. 653–661, Feb. 2013, doi: [10.1109/TED.2012.2225836](https://doi.org/10.1109/TED.2012.2225836).
- [9] Y. S. Chauhan, F. Krummenacher, R. Gillon, B. Bakeroot, M. J. Declercq, and A. M. Ionescu, "Compact modeling of lateral nonuniform doping in high-voltage MOSFETs," *IEEE Trans. Electron Devices*, vol. 54, no. 6, pp. 1527–1537, Jun. 2007, doi: [10.1109/TED.2007.896597](https://doi.org/10.1109/TED.2007.896597).
- [10] M. B. Willemsen and R. van Langevelde, "High-voltage LDMOS compact model for RF applications," in *Int. Electron Devices Meeting (IEDM) Tech. Dig.*, Washington, DC, USA, 2005, pp. 208–211, doi: [10.1109/IEDM.2005.1609308](https://doi.org/10.1109/IEDM.2005.1609308).
- [11] S. J. Sque, A. J. Scholten, A. C. T. Aarts, and D. B. M. Klaassen, "Threshold behavior of the drift region: The missing piece in LDMOS modeling," in *IEEE Int. Electron Devices Meeting (IEDM) Tech. Dig.*, Washington, DC, USA, 2013, pp. 336–339, doi: [10.1109/IEDM.2013.6724619](https://doi.org/10.1109/IEDM.2013.6724619).
- [12] Y. S. Chauhan, "Compact transistor modeling of high voltage MOSFETs," Ph.D. dissertation, Eng. Sci. Tech. Gen. Electron. Lab., EPFL, Lausanne, Switzerland, 2007.
- [13] A. W. Ludikhuizen, "Kirk effect limitations in high voltage IC's," in *6th Int. Symp. Power Semicond. Devices Ics Tech. Dig. (ISPSD)*, Davos, Switzerland, 1994, pp. 249–252, doi: [10.1109/ISPSD.1994.583734](https://doi.org/10.1109/ISPSD.1994.583734).
- [14] *HiSIM_HV 2.4.1 User's Manual*. Accessed: Mar. 2020. [Online]. Available: http://https://home.hiroshima-u.ac.jp/usdl/HiSIM_HV/index.html
- [15] G. Gildenblat *et al.*, "Surface-potential-based compact model of bulk MOSFET," in *Compact Modeling: Principles, Techniques and Applications*. G. Gildenblat, Ed. New York, NY, USA: Springer, 2010, ch. 1, pp. 3–40, doi: [10.1007/978-90-481-8614-3](https://doi.org/10.1007/978-90-481-8614-3).
- [16] K. Xia, C. C. McAndrew, R. van Langevelde, G. D. J. Smit, and A. J. Scholten, "Improved modeling of LDMOS with non-uniform lateral channel doping," in *Proc. Electron Devices Technol. Manuf. Conf.*, Singapore, 2019, pp. 124–125.
- [17] C. Gupta, H. Agarwal, R. Goel, C. Hu, and Y. S. Chauhan, "Improved modeling of bulk charge effect for BSIM-BULK model," *IEEE Trans. Electron Devices*, vol. 66, no. 6, pp. 2850–2853, Jun. 2019, doi: [10.1109/TED.2019.2910107](https://doi.org/10.1109/TED.2019.2910107).
- [18] K. Xia, "New c^∞ functions for drain-source voltage clamping in transistor modeling," *IEEE Trans. Electron Devices*, vol. 67, no. 4, pp. 1764–1768, Apr. 2020, doi: [10.1109/TED.2020.2974790](https://doi.org/10.1109/TED.2020.2974790).
- [19] P. Hower *et al.*, "A rugged LDMOS for LBC5 technology," in *Proc. 17th Int. Symp. Power Semicond. Devices ICs (ISPSD)*, Santa Barbara, CA, USA, 2005, pp. 327–330, doi: [10.1109/ISPSD.2005.1488017](https://doi.org/10.1109/ISPSD.2005.1488017).



KEJUN XIA (Senior Member, IEEE) received the Ph.D. degree in electrical engineering from Auburn University, Auburn, AL, USA, in 2006. From 2006 to 2014, he worked on SPICE modeling as a Senior Principal Member of Technical Staff with Maxim Integrated, Beaverton, OR, USA. From 2014 to 2019, he managed a device and product modeling team for NXP Semiconductors, Chandler, AZ, USA, where he currently manages a High Voltage and Analog Technology Development Team.



COLIN C. MCANDREW (Fellow, IEEE) received the B.E. (Hons.) degree in electrical engineering from Monash University, Melbourne, Australia, in 1978, the M.A.Sc. and Ph.D. degrees in systems design engineering from the University of Waterloo, Canada, in 1982 and 1984, respectively. From 1987 to 1995, he was with AT&T Bell Laboratories, Allentown, PA, USA. He is currently a Fellow with NXP Semiconductors, Chandler, AZ, USA.



RONALD VAN LANGEVELDE received the M.S. and Ph.D. degrees in electrical engineering from the Eindhoven University of Technology, The Netherlands, in 1994 and 1998, respectively. From 1998 to 2013, he worked with Philips Research, The Netherlands, in the fields of compact modeling for circuit simulation and analogue/RF IC-design. Since 2013, he has been worked with NXP Semiconductors, The Netherlands, as a Technical Director on spice modeling.